FRACTURE OF CEMENT AND CONCRETE

S. P. Shah

Department of Civil Engineering, Northwestern University, Evanston, IL 60201, USA

ABSTRACT

Various investigators have carried out tests to determine K_{Ic} values for portland cement mortar, concrete and fiber reinforced concrete. The value of K_{Ic} is generally derived from experimental values of the maximum load, the length of the premolded notch and the relevant LEFM formula. The reported values vary widely even for essentially similar materials. This apparent inapplicability of the conventional LEFM approach results from a substantial slow crack growth that occurs prior to peak load and a large nonlinear fracture process zone around the crack tip. Theoretical and experimental methods to include these nonlinear effects are described in this plenary paper. The method proposed considers the nonlinear coupling among the closing pressure in the fracture process zone, and the crack opening displacement and the specimen geometry, as well as the energy absorbed in the fracture process zone.

KEYWORDS

Portland cement; composites; fracture mechanics; nonlinear strain energy; plasticity; concrete; fiber reinforced concrete; microcracking; notched beams; double cantilever beams; double torsion beams; microscopy.

INTRODUCTION

The field of fracture mechanics originated in the 1920's with A. A. Griffith's work on fracture of brittle materials such as glass. Its most significant applications, however, have been for controlling brittle fracture and fatigue failure of metallic structures such as pressure vessels, airplanes, ships and pipelines. Considerable development has occurred in the last twenty years in modifying Griffith's ideas or in proposing new concepts to account for the ductility typical of metals. As a result of these efforts, standard testing techniques have been available to obtain fracture mechanics parameters for metals, and design based on these parameters are included in relevant specifications.

Many attempts have been made, in the last decade or so, to apply the fracture mechanics concepts to cement, mortar, concrete and fiber reinforced concrete. So far, these attempts have not led to a unique material parameter which can quantify the resistance of these cementitious composites to fracture. As a result of this difficulty in establishing fracture mechanics parameters, researchers and designers often ask whether the fracture mechanics concepts are valid for concrete, and whether the conventional strength of materials approach is not sufficient for the design of concrete structures.

To partly answer these questions, first a brief and somewhat superficial summary of the current brittle-fracture design considerations as developed for metallic materials is given (see Std. Methods... for complete review). Secondly, some of the difficulties in determining a valid fracture mechanics parameter for cementitious composites are examined. Some possible current research directions to obtain valid fracture mechanics parameters for concrete are indicated in the last part of the paper.

BRITTLE-FRACTURE DESIGN CONSIDERATIONS

It has been realized that under certain conditions of strain rate, temperature and constraint, many otherwise ductile structural steel fail in a brittle manner. This ductile-brittle transition characteristic for low and intermediate strength steels have been traditionally measured by various impact strengths. In such impact tests, the energy required to fracture a notched specimen (Charpy-V-Notch Specimen) is taken as a measure of notch-toughness. Although these notch-toughness tests are useful in delineating the service temperature range, the results which are expressed in terms of energy cannot always be translated into structural engineering and design parameters such as stress and flaw size. Fracture mechanics is a method of characterizing the fracture behavior in structural parameters that can be used directly by engineers. It is based on a stress analysis, flaw size and the material toughness.

In a linear elastic analysis of a two-dimensional symmetrical specimen, the stresses in the region of a crack tip in a body subjected to tensile stresses normal to the plane of the crack (Mode I deformation) can be expressed as

$$\sigma_x, \sigma_y = K_I r^{-\frac{1}{2}} f(\theta) \qquad (1)$$

Note that the function $f(\theta)$ does not depend on the specimen or the loading geometry. Consequently, it is reasonable to formulate failure criteria in terms of load and geometry dependent term K_I, the stress intensity factor.

One of the underlying principals of fracture mechanics is that unstable fracture occurs when the stress intensity factor at the tip of the crack reaches a critical value. This critical value is a material toughness property and also depends on loading rate and constraint as follows:

K_c = critical stress intensity factor for static loading and plane-stress conditions of variable constraint and depends on specimen thickness, crack size and the length of the uncracked ligament.

K_{Ic} = critical stress intensity factor for static loading and plane-strain conditions for maximum constraint (to plastic flow). This value is minimum for thick plates.

K_{Id} = critical stress intensity factor for dynamic loading and plain-strain conditions,

where

$$K_c, K_{Ic} \text{ and } K_{Id} = C\sigma\sqrt{a} \qquad (2)$$

C = a constant depending on specimen and crack geometry

σ = a nominal stress

a = flaw size

Each of these K values may also be a function of temperature.

By knowing the critical value of stress intensity factor for a particular thickness, loading rate and temperature, the designer can determine the flaw size that can be tolerated for a given design stress level, or he can determine the design stress level that can be tolerated for an existing crack that may be present in a structure.

EXPERIMENTAL DETERMINATION OF K_{Ic}

The critical value of stress intensity factor for metallic material is a thickness dependent property. Over a certain rage of thickness, the critical combination of load and crack length at instability (K_c) decreases with an increase in thickness reaching a rather constant minimum value (K_{Ic}). At the crack tip prior to crack extension, a plastic zone (fracture process zone) exists. The size of this zone is much larger at the surface of sheet specimens than at the center where the stresses in the perpendicular directions (σ_z) provide constraint to plastic flow. For thick specimens, the effects of triaxial stresses (plane-strain condition) is predominant and, as a result, crack extension takes place without any appreciable plastic flow. Thus, a minimum value toughness (K_{Ic}) is observed for sufficiently thick plate specimens.

If the length of the uncracked ligament is small compared to the size of the plastic zone, then elastic, plane-strain conditions are not possible. Some idea of the size of the plastic zone can be obtained by substituting $r = r_y$ and $\sigma_y = \sigma_{ys}$ in Equation (1). Thus, the radius of the plastic zone is proportional to the quantity $(K_I/\sigma_{ys})^2$, where σ_{ys} = the yield strength of the material.

To obtain a unique lower bound value of material fracture toughness for metals, specimens are specially designed to assure that plane-strain conditions exist during crack propagation. The test methods and the design of specimens are described in relevant ASTM specifications (for example, ASTM E-339). Two recommended test specimens are bend specimen and compact tension specimen. To assure elastic plane-strain behavior, the thickness of the specimen (B), the length of the crack (a) and the length of the uncracked ligament (W-a) should be substantially larger than the size of the plastic zone. This is assured by the following minimum specimen dimensions:

$$a, B \text{ and } (W - a) \geq 2.5\left(\frac{K_{Ic}}{\sigma_{ys}}\right)^2 \qquad (3)$$

These specifications assure that the specimen thickness, crack length and the length of the uncracked ligament are approximately 50 times the radius of the plastic zone. Note that if plane-strain conditions are not maintained, then the value of critical stress intensity factor (K_c) will not be unique for a given material, but will depend on the test specimen dimensions.

Various investigators have carried out tests to determine K_{Ic} values for portland cement, mortar, concrete and fiber reinforced concrete. The value of K_{Ic} is generally derived from experimental values of maximum load, the length of the premolded notch and the formulae derived from linear elastic fracture mechanics (LEFM) concepts. The reported values of K_{Ic} vary widely even for essentially similar materials as can be seen from Table 1 (Velazco, Visalvanich, Shah, 1980). There are two main reasons for this apparent inapplicability of the conventional procedure in determining the fracture toughness parameter. A substantial slow (or subcritical) crack growth occurs prior to the peak load. Unless this additional crack growth is accurately measured and accounted for, a specimen geometry independent fracture toughness parameter cannot be obtained. In addition to the slow crack growth, fracture in cement based composites is associated with a fracture process zone surrounding the crack tip. This nonlinear region is characterized by microcracking in front of and interlocking (due to roughness of the crack) behind the visible crack tip. Unlike a conventional Griffith crack, the traction forces across the crack in the fracture process zone is not zero.

Portland cement concrete is characterized by strain softening and nonlinear behavior and it is not clear that the testing specifications developed for metals can be applied to concrete. In addition, it has been shown that the nonlinear behavior of concrete is related to its heterogeneity; the larger the volume fraction of inclusions, the more nonlinear and tougher is the observed behavior (Shah, McGarry, 1971). Since fairly large grain size are used in making concrete (23mm), the extension of the formulae developed for metals would lead to extremely large size specimens.

An alternate approach is to modify the concepts of linear elastic fracture mechanics to include the effects of slow crack growth and crack-tip nonlinearity (process zone) in analysing the results of fracture toughness tests. This is attempted in this paper.

SLOW CRACK GROWTH

To limit the extent of slow crack growth ASTM-E399 specifies that the relationship between the measured load (p) and the crack mouth displacement (Δ) should be almost linear (Fig. 1). This is stipulated by specifying that the ratio of the maximum load (P_{max}) and P_5 (see Fig. 1, for definition) cannot be greater than 1.10 for a valid fracture toughness (K_{Ic}) test. In Fig. 1 is shown a load vs. crack mouth displacement record of a portland cement mortar notched beam specimen described in Fig. 2 (Velazco, Visalvanich, Shah, 1980). It can be seen that P_{max}/P_5 is much greater than 1.10. A substantial slow crack growth was observed during loading with the aid of a microscope (Velazco, Visalvanich, Shah, 1980). These results are for mortar specimens made with small grain size inclusions (sand particles). The extent of slow crack growth is likely to be even larger for concrete specimens which are made with larger size coarse aggregates.

Resistance Curves

If the slow crack growth is accurately measured then one can calculate load and strain energy release rate at each crack extension and obtain a relationship between the crack growth and the strain energy release rate. Such plots are called R-curves or resistance curves (Fig. 3). The resistance to crack extension as measured by the corresponding strain energy release rate (G_R) at first increases due to the slow crack growth and then reaches a steady state value (G_{ss}). The concept of R-curves to characterize the resistance during slow crack growth for rocks, ceramics, asbestos cement, mortar and concrete has been used by many investigators (Lenian, Bunsell, 1979; Mai, 1979; Schmidt, Lutz, 1978; Foote, Cottrell, Mai, 1980).

Measurement of Slow Crack Growth

To accurately measure the slow crack growth the specimens should be loaded at a constant rate of crack mouth displacement and the load stopped at frequent intervals for measurement of crack growth. Even with the stable loading arrangement, the measurement of crack growth in concrete can be difficult because of the opaque nature of the material, and the tortuosity of the crack growth.

An alternate method to obtain the extent of slow crack growth is by so-called compliance calibration technique. In this method, compliance of a previously artifically notched specimen is compared with the compliance of a specimen under test. Several investigators have used this approach to examine the slow crack growth (Lenian, Bunsell, 1979; Mai, 1979; Foote, Cottrell, Mai, 1980; Brown, 1972; Swartz, Hu, Jones, 1978; Cook, Crookham, 1978; Hillemier, Hilsdorf, 1971). However, with this method it is assumed that the compliance of a specimen with an artificial crack is identical to that of a specimen with a real crack. This is not the case in mortar and concrete because of the irregular and rough nature of real cracks (Velazco, Visalvanich, Shah, 1980; Cook, Crookham, 1978) Resulting from aggregate-interlock, these cracks have lower compliance than the artifically cast smooth cracks. Because of these difficulties, in the investigations carried out by the author, the crack growth is measured with an internally illuminated microscope which is fitted with a micrometer. This optical arrangement permits measurement of a crack with a resolution of 1.3×10^{-3} mm.

Measurement of Fracture Resistance

From the measurement of load and crack growth, the resistance to slow crack growth can be calculated using linear elastic fracture mechanics in terms of either stress intensity factor (K_R) or the strain energy release rate (G_R). This would be valid if the nonlinear effects around the crack tip resulting from microcracking ahead of the crack and the aggregate interlocking behind the crack were negligible. These effects, however, are substantial for mortar and concrete.

The significant extent of nonlinearity was observed in the load vs. load-line deflection curves for double cantilever and double torsion concrete specimens (Figs. 4, 5) (Wecharatana, shah, 1980, 1982). These specimens were loaded at a constant rate of crack opening displacement. The load was periodically stopped to measure crack growth (microscopically). The specimens were then unloaded and again loaded.

For the case of linearily elastic, brittle materials, the strain energy

release rate can be calculated from:

$$G_R = \frac{P^2}{2} \frac{dC}{dA} \tag{4}$$

where dC/dA is the rate of change of compliance with respect to crack growth. To obtain G_R using Eq. (4) during slow crack growth from the test results, one can calculate the changes in the values of secant compliances (C_s in Fig. 5) with the measured crack growth. This procedure cannot be very accurate for concrete since it ignores the effects of observed nonlinear deformation (δ_p) as shown in Fig. 5.

Many investigators use reloading (or unloading) compliance (C_R in Fig. 5) to calculate the value of G_R in Eq. (4) (Lenian, Bunsell, 1979; Brown, 1972; Hillemier, Hilsdorf, 1971). However, it was shown by the author (Shah, Wecharatana, 1980, 1982), that the use of reloading compliances to calculate G_R underestimates the fracture resistance for cementitious composites since that method ignores the inelastic energy absorbed during the crack growth. To include the inelastic energy during crack growth, the author has proposed modified definition of G_R as follows (Fig. 6).

$$\text{(Modified) } G_R = \frac{P_1 P_2}{2} \frac{dC_R}{dA} + \frac{(P_1 + P_2)}{P_1 P_2} \frac{d\delta_p^2}{dA} \tag{5}$$

where $d\delta_p/dA$ is the rate of change of permanent deformations with the crack growth and P_1, P_2 are two neighboring consecutive loads. Attempts to modify the linear elastic-fracture-mechanics definition of G_R has also been reported by Hodgkinson and Williams (1981) for polymeric materials.

R-curves calculated using Eq. (5) for mortar and concrete are shown in Fig. 3 (Wecharatana, Shah, 1982). It can be seen that the higher the maximum size of aggregates or volume fraction of aggregates, the higher is the value of fracture toughness as measured by R-curves. It should be noted that the conventional compressive strength of concrete specimens was lower than that of mortar specimens, but the values of the fracture toughness as measured by R-curves are higher for concrete specimens. On the other hand, the reported values of fracture toughness, calculated using LEFM, generally show direct relationship with the corresponding strength values.

PROCESS ZONE

To assure that the size of the test specimen is such that the dimensions of the process zone (plastic zone in metals) is relatively small so that the concepts of LEFM can be applied while calculating K_{Ic}, ASTM-E399 recommends that:

$$a, B, \text{ and } W - a \geq 2.5 \left[K_{Ic}/\sigma_{ys}\right]^2 \tag{6}$$

where a, b, and W are the length of the initial notch, the thickness of the specimen and the depth of the specimen, and σ_y is the yield strength of the material. This formula is based on the assumption that the size of the plastic zone is proportional to the quantity $(K_{Ic}/\sigma_{ys})^2$.

Attempts have been made to use the same concept for non-yielding material such as rocks and concrete. For example, Schmidt and Lutz (1978), showed that if the uniaxial tensile strength f_t is substituted for the yield strength σ_{ys} in Eq. (6) then the steady-state value of fracture toughness was obtained for rock specimens designed according to Eq. (6). The grain size of the rock specimens used by Schmidt and Lutz (1978), were 0.75mm. For that size, they found that a crack length of 100mm or greater is needed to obtain a fracture toughness value independent of crack length. For a much larger grain size in concrete, extremely large specimens would be necessary to obtain a steady state value of fracture toughness using Eq. (6).

A similar conclusion was also reached by Hillergorg, Modéer and Petersson (1976). They report that to have a valid test based on LEFM, notched beams should have a depth of 10 times a quantity which they term the characteristic length, l_{ch}, which is given by:

$$l_{ch} = \left(\frac{K_{Ic}}{f_t}\right)^2 \tag{7}$$

If their conclusion is valid, then one needs a depth of beams equal to 2 to 3 meters to obtain a steady-state value of fracture toughness for concrete.

The process zone in mortar and concrete is related to the aggregate interlock behind the crack tip. Thus, it seems likely that the size of this nonlinear zone should depend among other things, on size of the aggregate, the strength of the interface between the aggregates and matrix, and the geometry of the crack front. These factors are not included in Eq. (6) or (7). To consider these effects, a theoretical model was developed by the author (Wecharatana, Shah, 1983) to evaluate the length of the process zone. Unlike many previous models (Lenian, Bunsell, 1979; Foote, Cottrell, Mai, 1980; Dugdale, 1960), this model is not restricted to small-scale nonlinear zone.

The details of the theoretical model as well as detailed comparison with the experimental data are given in (Wecharatana, Shah, 1983a; Wecharatana, Shah, 1983b). A brief summary of the model is presented here. The model presented here is applicable to concrete as well as to fiber reinforced concrete.

BASIC CONCEPTS OF THE THEORETICAL MODEL

A crack just prior to its extension in Mode I opening in a fiber reinforced concrete specimen is shown in Fig. (7). The length of the crack can be divided into three regions: 1) a traction-free crack length which consists of initial cast notch and the zone of crack length where fibers are completely pulled out of the matrix, 2) the region of fiber bridging (δ_f), and 3) the matrix process zone (generally due to aggregate debonding and interlocking) in front of the crack tip. Both fiber bridging and matrix process zone provide resistance to crack opening. The effect of the fiber bridging is normally much more significant than that contributed from the matrix process zone, and as a result, the crack closing pressure in the matrix process zone can be neglected. On the other hand, in case of unreinforced matrix, there will not be any fiber bridging zone ($\delta_f = 0$).

Region 1 (traction-free crack) and Region 2 (fiber bridging) were separated

at the point where the crack surface displacement was equal to η^f_{max} (the maximum crack displacement where the fiber bridging stress is zero, since all fibers at that point are completely pulled out (Fig. 8) while the fiber bridging zone and the matrix process zone were separated at the point where crack surface displacement equalled to η^m_{max} (the maximum displacement of the matrix in the descending branch of the uniaxial tensile test where stress is equal to zero, Fig. (8).

The value of η^m_{max} has been reported by Wecharatana and Shah (1983a, 1983b). This value is about 0.8×10^{-3} in. for matrix mix 1:2:0:0.5 (C:S:A:W). The η^f_{max} value used in this study was half the fiber length. This may be justified (as shown in Fig. 8) from the observation that fibers are randomly distributed across the crack. The smallest pulled-out distance is equal to zero (labelled 3 in Fig. 8) and the largest pulled-out distance is half the fiber length (labelled 2 in Fig. 8). This implies that if the two crack surfaces are separated by a distance of half the fiber length, there will not be any fibers left bridging across the crack which subsequently means the fiber bridging pressure is zero.

If fibers are randomly distributed rather than aligned, then the maximum embedment length approaches $\ell/2$ in. Similarly, the η^m_{max} refers to the crack surface displacement where zero aggregate bridging and interlocking pressure is assumed (Fig. 8).

If the stresses in these nonlinear zones (fiber bridging and matrix process zone) are assumed to be purely under uniaxial tensile behavior, then crack length "a" can be replaced by an effective (elastic) crack "a_{eff}" such that $a_{eff} = a + \ell_p$, where ℓ_p is the idealized length of the matrix process zone (Fig. 7). This effective crack "a_{eff}" sustains two types of crack closing pressures: one due to the fiber bridging and another due to aggregate bridging. The concept of this model is somewhat similar to that originally proposed by Dugdale (1960) and Barenblatt (1962).

For a given applied load and an effective crack length, the crack opening process is primarily resisted by the bridging of fibers across the crack. It is necessary to first calculate the size of the fiber bridging zone. Since it is a function of the crack profile and the length of the fibers used, an approximate crack profile was first assumed (a linear crack profile was assumed in this study). Knowing the crack profile, crack length and η^f_{max} (half the fiber length), the size of fiber bridging zone was then determined. From the uniaxial tensile stress-displacement relationship and the assumed crack profile, the fiber bridging pressure can also be obtained. The stress displacement relationships are different for different fiber volume fraction and aspect ratio and for plain matrix. Details of how to obtain such relationships are described in Wecharatana and Shah (1983b).

In this analysis, it is assumed that crack will initiate as the crack surface displacement at the tip of the effective crack length "a" reaches a value η^m_{max} (defined in Figs. 7, 8).

As the fiber bridging pressure distribution depends on the crack surface displacement, which in turn is a function of the applied load, specimen geometry, the size of fiber bridging zone, the length of the matrix process zone ℓ_p and the closing pressure itself, an iterative procedure was then needed in the analysis as follows:

Consider a given crack length "a" in a fiber reinforced concrete specimen just prior to its further extension.

1. Assume a crack profile and a matrix process zone of length ℓ_p. With the given length of fibers used, the size of fiber bridging zone ℓ_f can be calculated using η^f_{max} as the limit of the fiber bridging zone.
2. Knowing ℓ_f and the assumed crack profile, calculate the closing pressure distribution, using the experimentally obtained stress-displacement relationship.
3. For a given specimen geometry (double cantilever beam, double torsion beam, and notched beam specimens were considered here), the applied load P and the crack closing pressure, calculate, using theory of elasticity, the crack opening displacements for the effective crack a_{eff}.
4. If the crack opening displacement at the end of matrix process zone (ℓ_p) is equal to η^m_{max}, then the initiation criterion is satisfied and the assumed value of ℓ_p is partially a correct one; otherwise a new value of ℓ_p is assumed and the above steps are repeated until the initiation condition is satisfied.
5. To further ensure that the iterated ℓ_p and the assumed crack profile are correct, the load line deformation (η_p) is calculated based on the same elastic principle and then compared with the experimentally observed values. If these values do not correspond to the measured data, a new crack profile is assumed and the above procedure is repeated until this condition is satisfied.

COMPARISON WITH EXPERIMENTAL DATA

The results of the analysis were compared with the data of notched beam tests reported by Velazco, Visalvanich, Shah, (1980), and the double cantilever beam tests reported by Wecharatana, Shah (1982) and Visalvanich, (1982) The notched beam specimens were 37.5mm wide (b), 75mm deep (w) and were tested in a four-point configuration with a distance between the load-point equal to 125mm (Figs. 2, 9). The length of the initial notch varied from 9mm to 37.5mm. The beams were reinforced with 1% by volume of smooth, steel fibers (ℓ = 25mm and d = .25mm). During loading, the crack length, the load-point deflection and the crack mouth displacement were continuously monitored.

The double cantilever beam specimens were 610mm long tapered beams developed by Visalvanich (1982), (Fig. 10). The crack plane had a thickness of 12.5mm. The beams were reinforced with smooth steel fibers (ℓ = 6 or 19mm, d = .15 or .4mm). The volume fraction of fibers varied from 0.5 to 2%. During loading, the crack extension and load-line deflections were measured.

The mortar matrix for both types of specimens had mix proportion by weight: 1:2:0.5. For this mortar the value of η^m_{max}, the critical crack opening

displacement was estimated from the data of Evans and Marathe as .02mm, (Wecharatana, Shah, 1983a)

A typical comparison of load-CMD curves for notched beam and the load-η_p curves for the double cantilever beam specimens is shown in Figs. 11 and 12. Theoretical plots of strain energy release rate vs. crack extension (R-curves) for the double cantilever beam specimens are shown in Fig. 13. The experimental R-curves were available for only one set of specimens; only these specimens were unloaded and reloaded after each observation of crack extension. The comparison between theoretical and experimental results is judged satisfactory.

Note that if the asymptotic value of the R-curve is considered a material parameter, then that value can be a useful quantity in identifying the benefits of fiber addition. For example, the steady state asymptotic value of specimens reinforced with 19mm fibers is approximately 40 times that for plain, unreinforced matrix (Fig. 13). This relative improvement in fracture energy is comparable to the reported value of "toughness index" (relative values of the areas under the load-deflection curves in flexure), (Henager, 1978).

MATRIX PROCESS ZONE, FIBER BRIDGING ZONE AND CRITICAL COD

The value of the matrix process zone ℓ_p can only be obtained through the interation procedure which must satisfy the initiation criterion that the crack tip opening displacement equals η^m_{max} used here for the matrix was 0.08×10^{-2} in., as reported by Wecharatana, Shah (1983a), Wecharatana, Shah (1983b). The fiber bridging zone was calculated from the assumed crack profile with the condition that fibers will be completely pulled out when the crack surface displacement equals η^f_{max} (half the fiber length, Fig. 8). In this study, since the value of crack opening displacement was always less than η^f_{max} (half the fiber length), the size of the fiber bridging zone was then equal to the crack length subtracted by the length of the initial cast notch.

Fig. 14 shows the plot of both the calculated matrix process zone and the fiber bridging zone (ℓ_p and ℓ_f, respectively) for the DCB specimens. It can be observed that the matrix process zone is essentially constant with respect to crack growth. The value of ℓ_p calculated from fiber reinforced mortar specimen was almost identical to those obtained from mortar specimens by Wecharatana, Shah (1983a), and Wecharatana, Shah (1983b). The conclusion of constant process zone has been also confirmed in other materials like DMMA (Döll, Weiman, 1979), and (Schinker, Döll, 1979). The obtained value of ℓ_p was found to be approximately about 3 in. and seemed to be independent of different fiber volume fraction and aspect ratio (Fig. 14).

A plot of the matrix process zone and the fiber bridging zone with the uncracked ligament in the notched beam specimens is shown in Fig. 15. The predicted matrix process zones, using the proposed model, were found close to what has been reported for the unreinforced moartar (Wecharatana, Shah, 1983a; Wecharatana, Shah, 1983b). Fig. 15 also shows that the fiber bridging zone increases as the uncracked ligament decreases.

CONCLUSIONS

Classical linear elastic fracture mechanics analysis is modified to predict fracture energy (R-curves) for cement based compsites. The predicted results compare well with the experimental data of DCB and NB specimens. The size of the fracture process remains constant during the slow crack growth, but it depends on the geometry of the specimen. Unless this variation is considered, R-curves will not be specimen geometry independent. The proposed model provides a method to calculate fracture resistance of a crack in a specimen of any geometry. Calculations of crack opening displacements were based on simple but approximate analysis and are currently being further refined at Northwestern University (Ballarini, Shah, Keer, 1984). One of the key parameters in the model is the relationship between uniaxial post-cracking stress and the corresponding displacement. This relationship will depend on the material microstructure. Experiments to determine this relationship for a variety of composites are currently underway at Northwestern University.

ACKNOWLEDGMENT

The research reported here is being supported by grants from the National Science Foundation and Air Force Office of Scientific Research to Northwestern University.

REFERENCES

Ballarini, R., S. P. Shah, and L. M. Keer, (1984). Crack Growth in Concrete Based Composites. To be published in Engineering Fracture Mechanics.

Barenblatt, G. J., (1962). The Mathematical Theory of Equilibrium Crack in the Brittle Fracture. Advances in Applied Mechanics, Vol. 7, pp. 55-125.

Brown, J. H., (1972). Measuring the Fracture Toughness of Cement Paste and Mortar. Magazine of Concrete Research, Vol. 24, No. 81, pp. 185-196.

Cook, D. J., and G. D. Crookham (1978). Fracture Toughness Measurements of Polymer Concrete. Magazine of Concrete Research, Vol. 30, No. 105, pp. 205-214.

Doll, W. and G. W. Weiman (1979). Deformationsverhalten von PMMA Crazes an Ribspitzen. Progress in Colloid and Polymer Science, Vol. 66, pp. 291-298.

Dugdale, D. S. (1960). Yielding of Steel Sheets Containing Slits. Journal of Mechanics, Physics and Solids, Vol. 8, pp. 100-104.

Foote, R. M., B. Cottrell, and Y. W. Mai (1980). Crack Growth Resistance Curve for a Cement Composite. Advances in Cement-Matrix Composites, Proceedings, Symposium L, Materials Research Society, Annual Meeting, Boston, Massachusetts, pp. 95-106.

Henager, C. H. (1978). A Toughness Index for Fiber Concrete. RILEM Symposium, Sheffield, pp. 79-86.

Hillemier, B., and H. K. Hilsdorf (1971). Fracture Mechanics Studies on Concrete Composites. Cement and Concrete Research, Vol. 7, pp. 523-536.

Hillerborg, A., M. Modéer, and P. E. Petersson (1976). Analysis of Crack Formation and Crack Growth in Concrete by Means of Fracture Mechanics and Finite Elements. Cement and Concrete Research, Vol. 6, pp. 773-782.

Hodgkinson, J. M., and J. G. Williams (1981). J and G_c Analysis of the Tearing of Highly Ductile Polymer. Journal of Materials Science, Vol. 16, pp. 50-56.

Lenian, J. C., and A. R. Bunsell (1979). The Resistance to Crack Growth of Asbestos Cement. Journal of Materials Science, Vol. 14, pp. 321-332.

Mai, Y. W., (1979). Strength and Fracture Properties of Asbestos Cement Mortar Composites. Journal of Materials Science, Vol. 14, No. 9,

pp. 2091-2102.

Schinker, M. G., and W. Doll (1979). Interference Optical Measurements of Large Deformations at the Tip of a Running Crack in a Glassy Thermoplastic. In J. Harding (Ed.), Mechanical Properties of Materials at High Rates of Strain. Inst. Phys. Conf. Ser., No. 47, Chapter 2, pp. 224-232.

Schmidt, R. A., and T. J. Lutz (1978). K_{Ic} and J_{Ic} of Westerly Granite — Effects of Thickness and In-Plane Dimensions. Fracture Mechanics Applied to Brittle Materials, ASTM-STP 678, ASTM, Philadelphia, pp. 166-182.

Shah, S. P., and F. J. McGarry (1971). Griffith Fracture Criteria and Concrete. Proceedings of ASCE, Journal of Engineering Mechanics Division, Vol. 47, No. EM6, pp. 1633-1676.

Standard Method of Test for Plane-Strain Fracture Toughness of Metallic Materials. ASTM Designation E399.74, Part 10, ASTM Annual Standard.

Swartz, S. E., K. K. Hu, and G. L. Jones (1978). Compliance Monitoring of Crack Growth in Concrete. Proceedings of ASCE, Journal of Engineering Mechanics Division, Vol. 104, No. EM4, pp. 789-800.

Velazco, G., K. Visalvanich, and S. P. Shah (1980). Fracture Behavior and Analysis of Fiber Reinforced Concrete Beams. Cement and Concrete Research, Vol. 10, pp. 41-51.

Visalvanich, K., (1982). Fracture Modelling for Fiber Reinforced Concrete. Ph.D. Dissertation, Dept. of Materials Engineering, University of Illinois at Chicago.

Wecharatana, M., and S. P. Shah (1980). Double Torsion Tests for Studying Slow Crack Growth of Portland Cement Mortar. Cement and Concrete Research, Vol. 10, pp. 833-844.

Wecharatana, M., and S. P. Shah (1982). Slow Crack Growth in Cement Composites. Proceedings of ASCE, Journal of Structural Division.

Wecharatana, M., and S. P. Shah, (1983a). Prediction of Nonlinear Fracture Process Zone in Concrete. Engineering Mechanics Division, Journal of the American Society of Civil Engineers.

Wecharatana, M., and S. P. Shah (1983b). A Model for Predicting Fracture Resistance of Fiber Reinforced Concrete. Vol. 13, No. 6, pp. 819-829.

Comparison of Critical Stress Intensity Factors ($MNm^{-3/2}$)

Investigators Year of Reports Type of Testing	Cement Paste	Mortar	Concrete	Steel Fiber Reinforced Concrete		
				V_f = 0.5%	V_f = 1%	V_f = 2%
Nishioka, et al. 1978 3-BD	---	---	0.73	---	1.47-1.76	1.42-1.71
4-BD	---	---	0.73	---	1.42-1.71	1.86-2.01
Mindess, et al. 1977 4-BD	0.49-0.66	---	0.87	0.75-0.90	0.85-1.06	1.00-1.31
Gjorv, et al. 1977 3-BD	0.09-0.11	0.16-0.2	0.07-0.24	---	---	---
Hillemeir, et al. 1977 CT	0.31	0.37	---	---	---	---
Brown, et al. 1973 4-BD	0.3	0.65-0.9	---	---	---	---
DCB	0.43	0.60-1.1	---	---	---	---
Harris, et al 1972 3-BD Dry	---	0.4	---	---	---	0.43
Wet	---	0.41				0.57
Kesler, et al. 1972 CCP	0.14-0.25	0.4-1.2	0.5-1.4	---	---	---
Velazco, et al. 1980	---	0.5	---	0.6	0.9-1.3	2.4

3-BD = 3 Points Bending 4-BD = 4 Points Bending CT = Compact Tension

DCB = Double Cantilever Beam CCP = Center-Cracked Plate Under Tension

Table 1

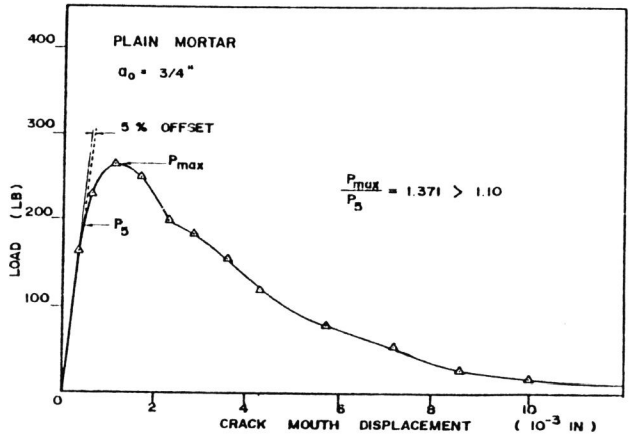

Fig. 1 - Slow Crack Growth in Mortar

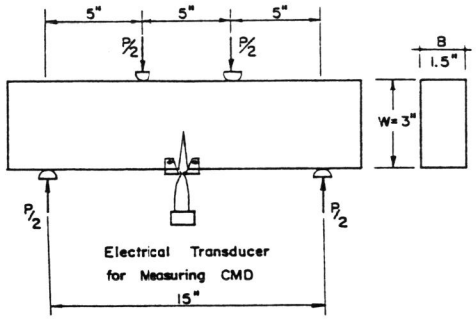

Fig. 2 - Dimensions of Notched Beam Specimens

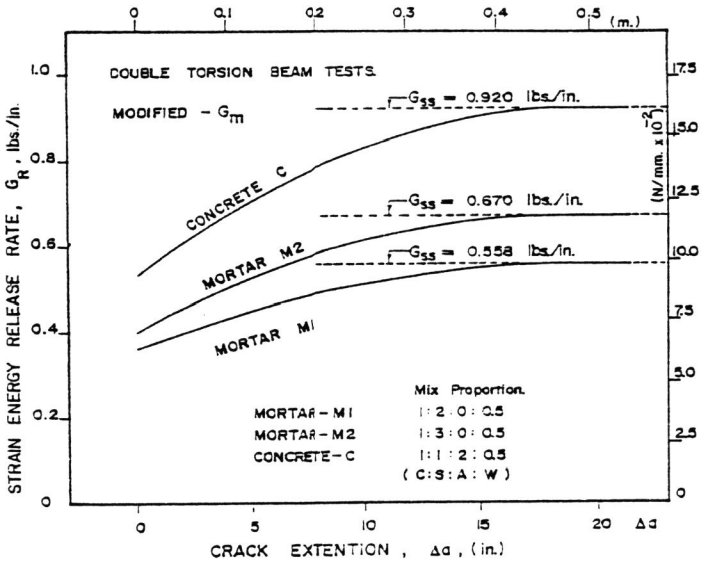

Fig. 3 - Examples of R-Curves

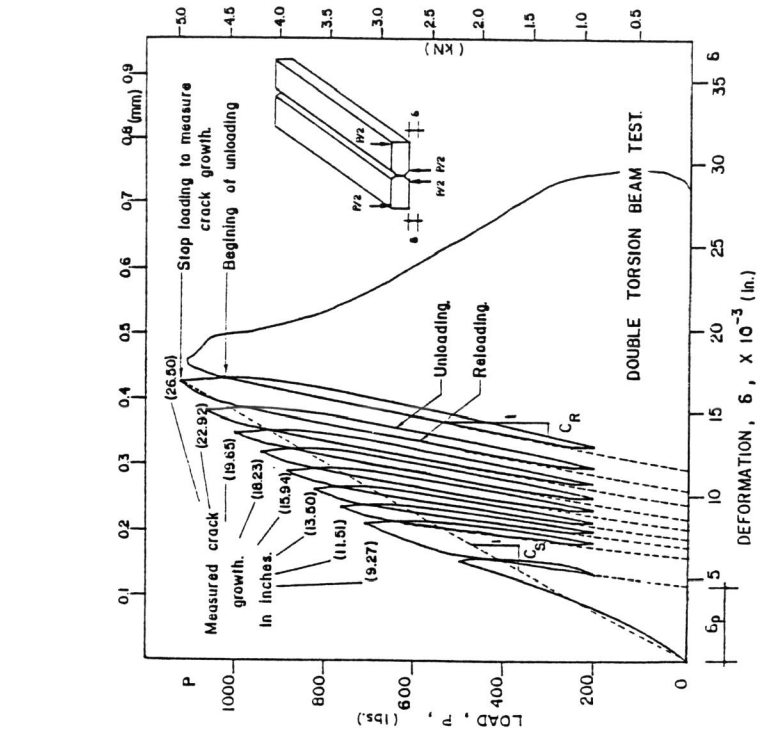

Fig. 5 - Typical Results from the Tests on DT Specimens

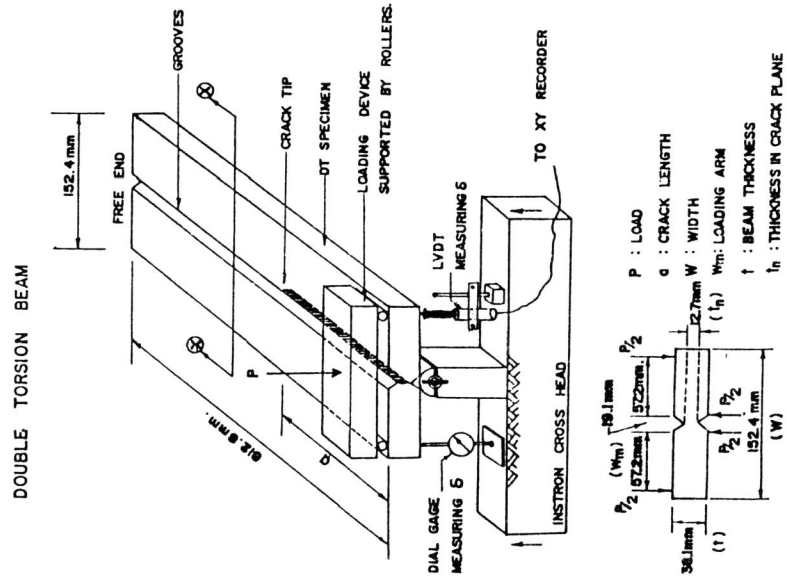

Fig. 4 - Dimensions of Double Torsion Beam Specimens

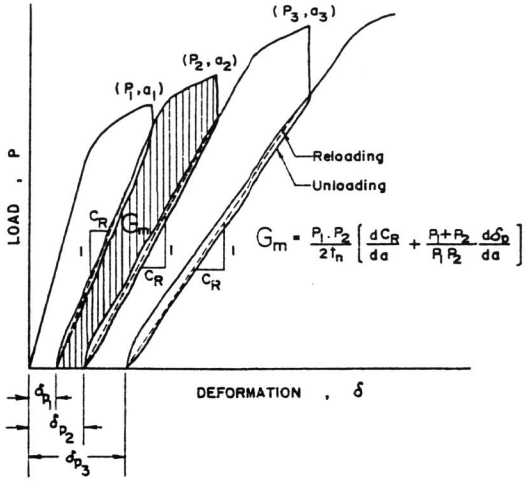

Fig. 6 - A New Method of Defining Strain Energy Release Rate.

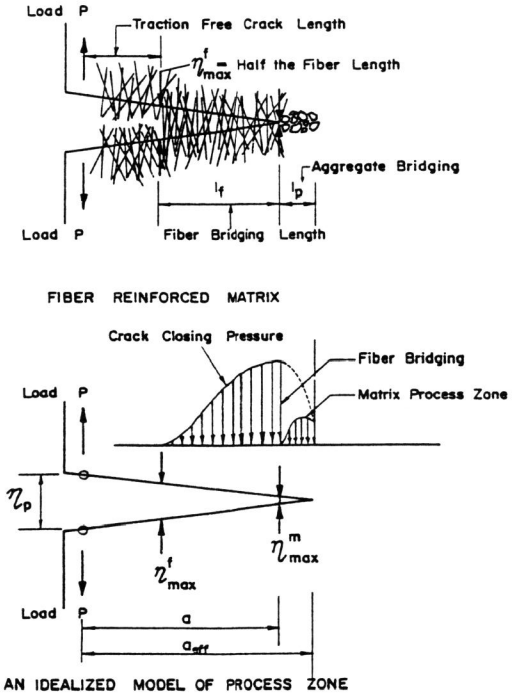

Fig. 7 - A Theoretical Model

(Below) Fig. 9 - The Proposed Model for Notched Beams

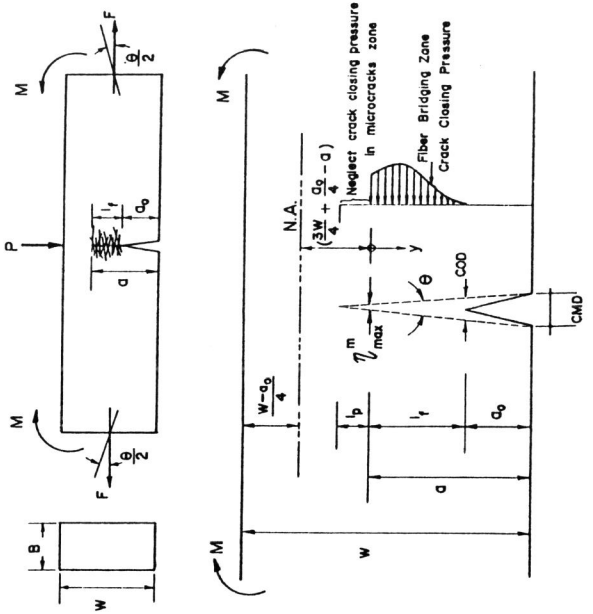

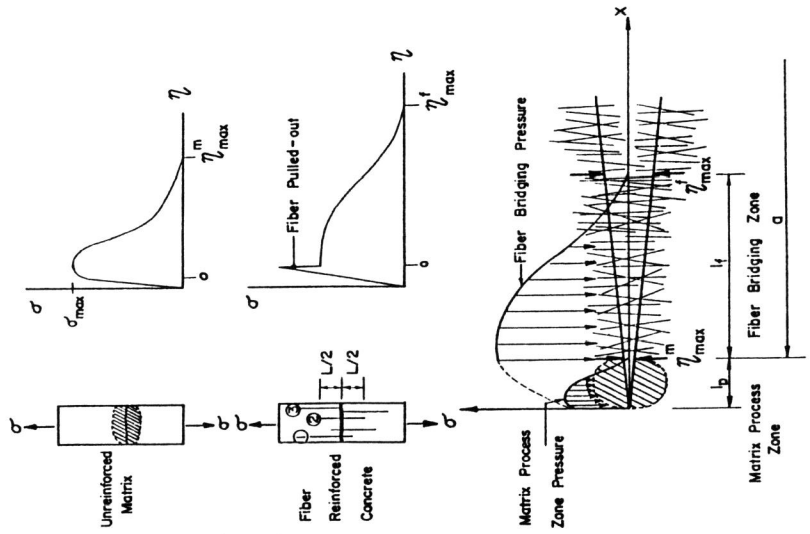

(Left) Fig. 8 - Relationships Between Crack Closing Pressure and Crack Opening Displacement in the Process Zone and Fiber Bridging Zone.

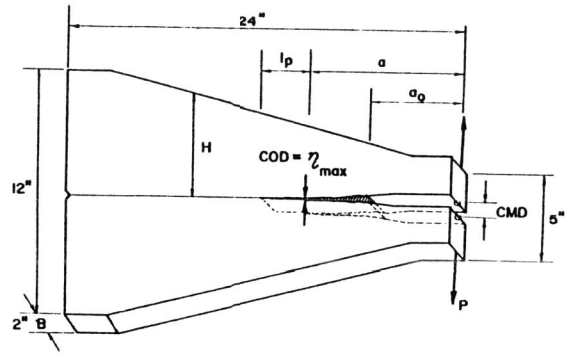

Fig. 10 - Application of the Theoretical Model for the DCB Specimen.

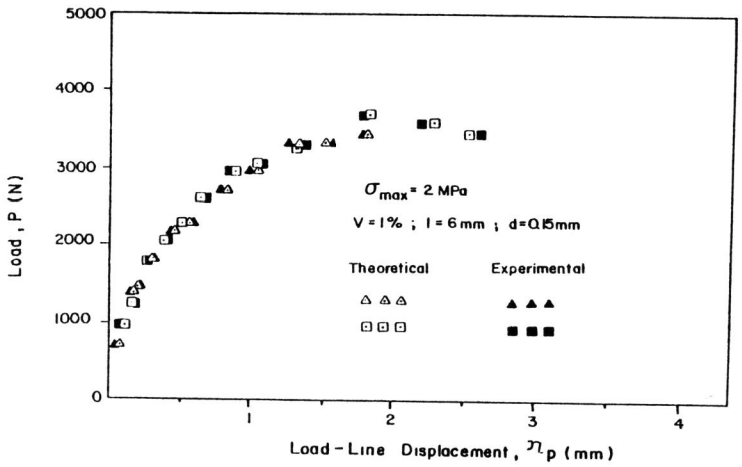

Fig. 11 - Theoretical Predictions for the DCB Specimens

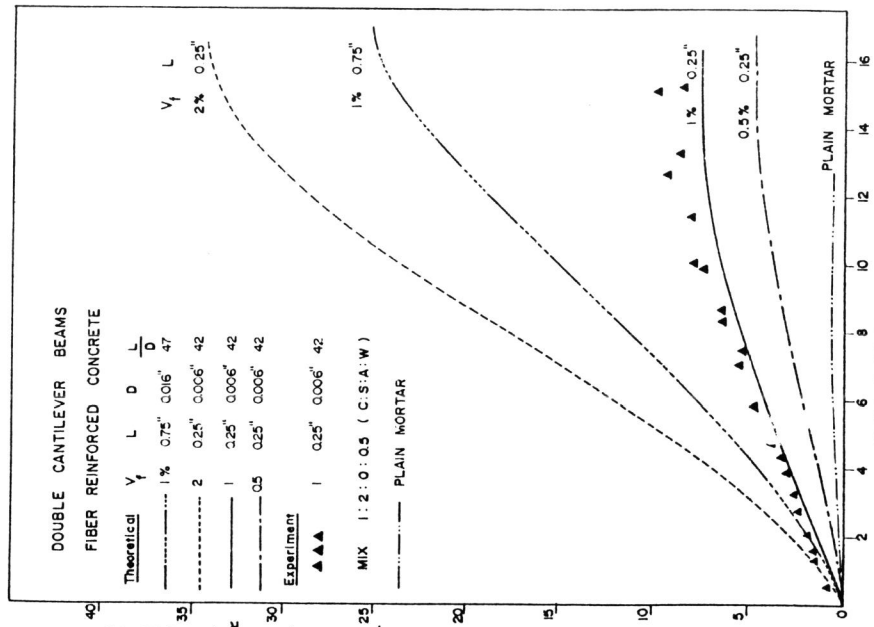

Fig. 13 - Theoretical R-Curves

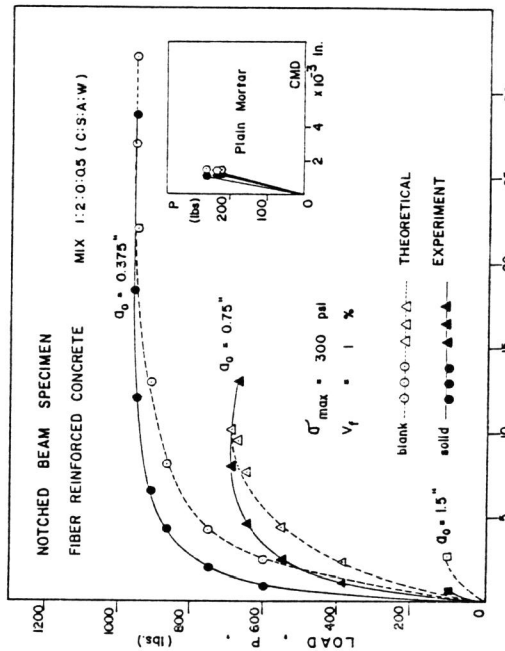

Fig. 12 - Theoretical Predictions for NB Specimen

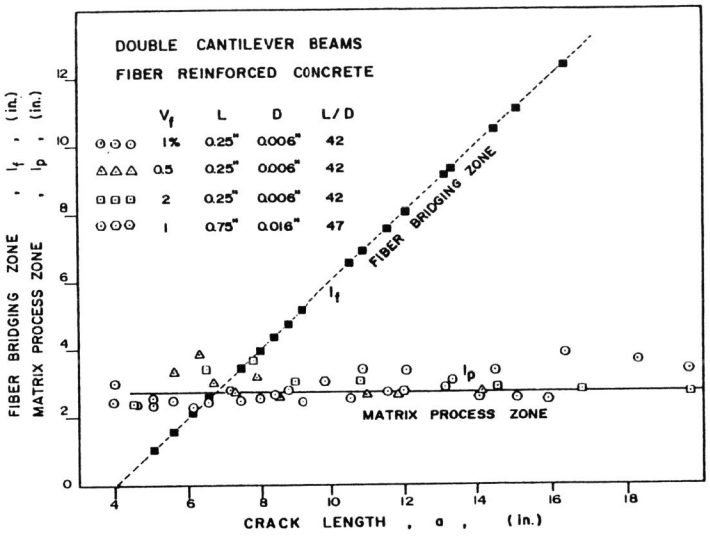

Fig. 14 - Predictions of the Length of the Process Zone

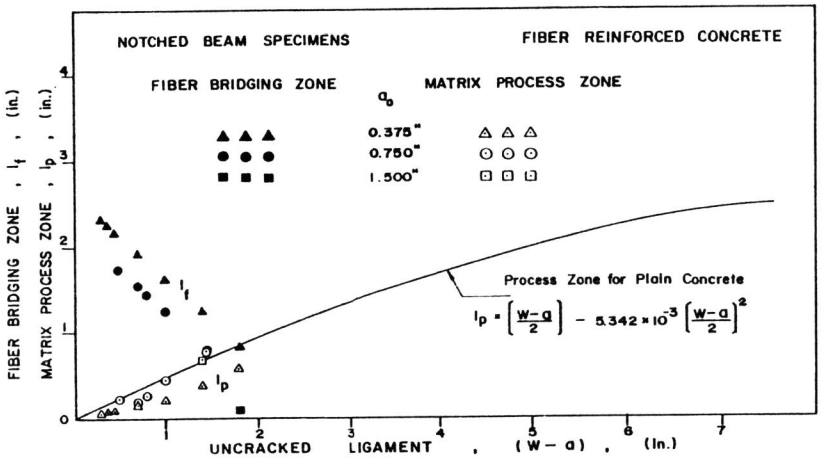

Fig. 15 - Variation of the Size of the Process Zone With the Size of the Beams.